Modelling of Electrostatics and Transport in GaN-Based HEMTs under Non-Equilibrium Conditions

Ivan Berdalović*, Mirko Poljak*, Tomislav Suligoj*
*Micro and Nano Electronics Laboratory, Faculty of Electrical Engineering and Computing,
University of Zagreb, 10000 Zagreb, Croatia
E-mail: ivan.berdalovic@fer.hr

***Abstract*—High electron mobility transistors (HEMTs) consisting of GaN and its alloys, most commonly AlGaN, have been gaining popularity as the next generation of high-speed devices for radiofrequency and power applications. Although a high concentration of 2D electrons in such structures can be obtained even in equilibrium, i.e. with a zero gate bias, in recent years there has been a tendency of developing normally-off, i.e. enhancement-mode GaN HEMTs to ease integration with the associated gate-driver circuitry. Therefore, accurate simulation of key electrical properties of these devices, such as electron mobility, becomes important even in non-equilibrium conditions, i.e. with an applied gate bias. This paper describes a simulation framework designed to enable the modelling of 2DEG mobility in enhancement-mode HEMTs. Apart from the Schrödinger and Poisson equations which need to be solved for the equilibrium case, the current continuity equations for electrons and holes also need to be satisfied when a positive gate bias is applied. All these equations are solved in a self-consistent numerical procedure to obtain a correct solution of the electrostatic problem for an arbitrary gate bias, as well as the discrete states and carrier wavefunctions needed for semi-classical mobility calculations. The procedure is demonstrated by simulating an advanced enhancement-mode device with a p-GaN cap and comparing the calculated electron concentrations and mobilities with available experimental results.**

Keywords*—*Radiofrequency integrated circuits, power semiconductor devices, quantum well devices, gallium nitride, high electron mobility transistors, heterojunctions, two-dimensional electron gas, semiconductor device modelling, charge carrier mobility

I. Introduction

The GaN material system has been one of the most exciting areas of research for radiofrequency (RF) and power electronics in recent years, owing to some of the unique advantages it offers compared to other semiconductors. Its wide bandgap means that high breakdown voltages and low leakage currents can be achieved, while the high saturation velocity and high mobility in GaN-based heterostructures are all beneficial for high-frequency operation. Another important property of material systems consisting of GaN and its alloys, typically AlGaN, is the high spontaneous and piezoelectric polarisation, resulting in high values of positive polarization sheet charge in the order of 10^{13} cm^{-2} at an AlGaN/GaN heterointerface [1]. As a consequence, a high concentration of electrons, a so-called 2D electron gas (2DEG), can be induced near the interface even without intentional doping. These electrons form the conducting channel of a GaN high electron mobility transistor (HEMT).

Most studies related to the electrical properties of GaN-based HEMTs have been limited to the equilibrium case, i.e. when a zero gate voltage is applied [2]–[7]. Since at that point the 2DEG is already formed in a typical AlGaN/GaN HEMT and the transistor is already "switched on", these studies are extremely useful in assessing the performance of these devices. However, for more advanced enhancement-mode device structures, where a positive gate voltage needs to be applied to turn the device on, only a limited number of studies pertaining to e.g. the electron mobility exists in the literature [8], [9]. One of the reasons could be that the Schrödinger-Poisson solvers traditionally used in these types of analyses are in general incapable of providing solutions to electrostatic problems far from equilibrium, as they assume a constant quasi-Fermi level across the entire vertical cross-section of the HEMT structure, an assumption which, strictly speaking, holds only in equilibrium. To simulate the behaviour of these devices at high applied gate voltages, the position-dependent quasi-Fermi levels need to be obtained by solving the current continuity equations alongside the Schrödinger and Poisson equations.

This paper presents a numerical implementation of a 1D simulator for MATLAB which solves the Schrödinger, Poisson and continuity equations in a self-consistent manner. The procedure to obtain the correct electrostatic solution for arbitrary GaN-based HEMT structures and for arbitrary gate biases is described. The simulator is coupled with a comprehensive mobility calculator which performs semi-classical calculations of the 2DEG mobility by solving the Boltzmann transport equation (BTE) in the momentum relaxation time approximation (MRTA), taking into account all relevant scattering mechanisms [10]. The need for such a complex simulation framework is demonstrated by simulating the electrostatics of an advanced enhancement-mode HEMT structure with a p-GaN cap at positive gate voltages. Finally, mobility calculations on such a device are performed and compared to available experimental data.

This work was supported by the Croatian Science Foundation (HRZZ) under the project IP-2018-01-5296.

II. Self-consistent solution of the electrostatic problem

A. Poisson equation

To obtain the electrostatic potential $V(z)$ for a given charge distribution $\rho(z)$, one needs to solve the 1D Poisson equation:

$$\frac{\partial^2 V(z)}{\partial z^2} = -\frac{\rho(z)}{\varepsilon(z)}. \tag{1}$$

After linearisation and discretisation on a uniform mesh with a mesh spacing Δ [11], taking into account the spatial variations of the dielectric constant $\varepsilon(z)$, the Poisson equation can be written as:

$$\begin{aligned}\frac{\varepsilon_{i-1}}{\Delta^2}V_{i-1} - \frac{(\varepsilon_{i-1}+\varepsilon_{i+1})}{\Delta^2}V_i + \frac{\varepsilon_{i+1}}{\Delta^2}V_{i+1} = \\ = -q\left(-n_i + p_i + N_i^d - N_i^a + N_i^p\right),\end{aligned} \tag{2}$$

where n_i and p_i denote the concentration of free carriers (electrons and holes) at mesh node i, N_i^d and N_i^a are the concentrations of ionised donors and acceptors, respectively, while N_i^p is the total polarisation charge appearing at material interfaces, which is calculated according to [12].

The desired boundary conditions for the conduction band without band offsets are applied as the boundary conditions for the potential. For mesh node 1, which is the node at the gate contact, this constitutes a Dirichlet boundary condition, and in the case of an Ohmic contact, V_1 is chosen to maintain charge neutrality, i.e. such that the carrier concentrations at the contact are equal to their equilibrium concentrations. In the case of a Schottky contact, V_1 is simply set as $V_G - \varphi_b^n$, where V_G is the applied gate voltage and φ_b^n is the Schottky barrier height, which is defined as the energy difference (in eV) between the equilibrium Fermi level and the conduction band, regardless of the semiconductor doping. For the potential at the last mesh node, V_N, either a Dirichlet condition enforcing charge neutrality or a Neumann boundary condition ensuring that the derivative of the potential is equal to zero can be applied.

B. Continuity equations

To obtain the quasi-Fermi levels used in the calculation of the carrier concentrations, one has to solve the continuity equations for the electron and hole current, which in one dimension and in steady-state conditions read:

$$\frac{\partial J_n}{\partial z} = qR, \tag{3a}$$

$$\frac{\partial J_p}{\partial z} = -qR, \tag{3b}$$

with q being the elementary charge and R being the net generation-recombination rate, which is often assumed to be zero when simulating transistor structures. Within the drift-diffusion model, the current densities can be expressed as:

$$J_n(z) = q\mu_n(z)n(z)\frac{\partial E_{Fn}}{\partial z}, \tag{4a}$$

$$J_p(z) = q\mu_p(z)p(z)\frac{\partial E_{Fp}}{\partial z}, \tag{4b}$$

where $\mu_{n,p}(z)$ is the electron/hole mobility, $n(z)$ and $p(z)$ are once again the electron and hole concentrations, respectively, while $E_{Fn,p}$ are the quasi-Fermi levels in electronvolts. To solve the continuity equations in a way that is numerically stable, they are discretised using the well-known Scharfetter-Gummel scheme [13], in which the current is expressed at the midpoints between mesh nodes. Assuming Boltzmann statistics (i.e. non-degenerate conditions) and a linear variation of the potential between adjacent mesh points, and assuming that the Einstein relation $D_{n,p} = \mu_{n,p}V_t$ holds, the electron and hole currents at the point $(i+1/2)$ over a uniform mesh can be written as [14]:

$$\begin{aligned}J^n_{i+\frac{1}{2}} = \frac{q}{\Delta}D^n_{i+\frac{1}{2}}N^c_{i+\frac{1}{2}}\left(\frac{V_i - V_{i+1}}{V_t}\right)\times \\ \times\frac{\left[\exp\left(\frac{E^{Fn}_{i+1}}{V_t}\right) - \exp\left(\frac{E^{Fn}_{i}}{V_t}\right)\right]}{\exp\left(-\frac{V_{i+1}}{V_t}\right) - \exp\left(-\frac{V_i}{V_t}\right)},\end{aligned} \tag{5a}$$

$$\begin{aligned}J^p_{i+\frac{1}{2}} = \frac{q}{\Delta}D^p_{i+\frac{1}{2}}N^v_{i+\frac{1}{2}}\left(\frac{V_{i+1} - V_i}{V_t}\right)\times \\ \times\frac{\left[\exp\left(-\frac{E^{Fp}_{i+1}}{V_t}\right) - \exp\left(-\frac{E^{Fp}_{i}}{V_t}\right)\right]}{\exp\left(\frac{V_{i+1}}{V_t}\right) - \exp\left(\frac{V_i}{V_t}\right)},\end{aligned} \tag{5b}$$

where $N_{c,v}$ represents the effective density of states of the conduction/valence band, and the diffusion coefficients $D_{n,p}$ are taken as constant within a given material. By introducing the Slotboom variables [15],

$$\Phi^n_i = \exp\left(\frac{E^{Fn}_i}{V_t}\right), \tag{6a}$$

$$\Phi^p_i = \exp\left(-\frac{E^{Fp}_i}{V_t}\right), \tag{6b}$$

equations (5a) and (5b) can be rewritten as:

$$\begin{aligned}J^n_{i+\frac{1}{2}} = \frac{q}{\Delta}D^n_{i+\frac{1}{2}}N^c_{i+\frac{1}{2}}\exp\left(\frac{V_i}{V_t}\right)B\left(\frac{V_i - V_{i+1}}{V_t}\right)\times \\ \times\left(\Phi^n_{i+1} - \Phi^n_i\right) = A^{n+}_i B^-_{i+1}\left(\Phi^n_{i+1} - \Phi^n_i\right),\end{aligned} \tag{7a}$$

$$\begin{aligned}J^p_{i+\frac{1}{2}} = \frac{q}{\Delta}D^p_{i+\frac{1}{2}}N^v_{i+\frac{1}{2}}\exp\left(-\frac{V_i}{V_t}\right)B\left(\frac{V_{i+1} - V_i}{V_t}\right)\times \\ \times\left(\Phi^p_{i+1} - \Phi^p_i\right) = A^{p+}_i B^+_i\left(\Phi^p_{i+1} - \Phi^p_i\right),\end{aligned} \tag{7b}$$

where $B(x) = x/[\exp(x) - 1]$ is the Bernoulli function. For small values of x, the well known approximation

$B'(x) = 1 - x/2$ [16] can be used instead of $B(x)$, thereby avoiding the singularity in $x = 0$ and making the calculation of the currents robust in case the electrostatic potential varies slowly across certain regions of the device. The above expressions constitute a version of the so-called Slotboom formulation of the Scharfetter-Gummel discretisation scheme for the continuity equations. To simplify the notation, the shorthand $A_i^{n,p+}$ has been introduced for the factors multiplying the Bernoulli function and the Slotboom variables, while B_{i+1}^- and B_i^+ represent the respective Bernoulli functions themselves.

Similar expressions for the electron and hole current at the mesh midpoints $(i-1/2)$ can be written by replacing $(i+1)$ with $(i-1)$ and placing a negative sign in front of (7a) and (7b). In the resulting expressions, one can denote the terms multiplying the Slotboom variables as $A_i^{n-}B_{i-1}^+$ and $A_i^{p-}B_i^-$. Then, using $(\partial J_{n,p}/\partial z)_i = \left(J_{i+1/2}^{n,p} - J_{i-1/2}^{n,p}\right)/\Delta$, one obtains a tridiagonal matrix equation for the Slotboom variable for both carrier types:

$$\frac{A_i^{n-}}{\Delta}B_{i-1}^+\Phi_{i-1}^n - \left(\frac{A_i^{n-}}{\Delta}B_{i-1}^+ + \frac{A_i^{n+}}{\Delta}B_{i+1}^-\right)\Phi_i^n + \\ + \frac{A_i^{n+}}{\Delta}B_{i+1}^-\Phi_{i+1}^n = qR, \tag{8a}$$

$$\frac{A_i^{p-}}{\Delta}B_i^-\Phi_{i-1}^p - \left(\frac{A_i^{p-}}{\Delta}B_i^- + \frac{A_i^{p+}}{\Delta}B_i^+\right)\Phi_i^p + \\ + \frac{A_i^{p+}}{\Delta}B_i^+\Phi_{i+1}^p = -qR. \tag{8b}$$

If R is taken as zero, only the boundary condition terms appear at the RHS of the matrix equations (8a) and (8b). Having obtained the Slotboom variables Φ_n and Φ_p, the quasi-Fermi levels E_{Fn} and E_{Fp} are easily obtained using (6a) and (6b).

For the quasi-Fermi levels at the gate contact, a simple Dirichlet boundary condition can be used in the case of an Ohmic contact, stating that $E_1^{Fn} = E_1^{Fp} = -V_G$. For a Schottky contact, it is common to assume that the current between the first two mesh points depends on the surface recombination velocities $v_{n,p}$:

$$J_{\frac{3}{2}}^n = -qv_n\left(n_1 - n_0\right), \tag{9a}$$

$$J_{\frac{3}{2}}^p = qv_p\left(p_1 - p_0\right), \tag{9b}$$

where n_1 and p_1 are the carrier concentrations at node 1, while n_0 and p_0 are the equilibrium concentrations for a given Schottky barrier height [17]. This translates to the following boundary condition for the Slotboom variables:

$$-\left(\frac{A_1^{n+}}{\Delta}B_2^- + \frac{v_n}{\Delta}\right)\Phi_1^n + \frac{A_2^{n-}}{\Delta}B_1^+\Phi_2^n = -v_n\frac{A_1^{n+}}{D_{\frac{3}{2}}^n}\Phi_0^n, \tag{10a}$$

$$-\left(\frac{A_1^{p+}}{\Delta}B_1^+ + \frac{v_p}{\Delta}\right)\Phi_1^p + \frac{A_2^{p-}}{\Delta}B_2^-\Phi_2^p = -v_p\frac{A_1^{p+}}{D_{\frac{3}{2}}^p}\Phi_0^p, \tag{10b}$$

with $\Phi_0^{n,p} = 1$. For simplicity, we assume a constant recombination velocity regardless of the gate bias [18]: $v_{n,p} = \sqrt{k_BT/2\pi m_{n,p}^*}$, $m_{n,p}^*$ being the effective mass of carriers. On the other hand, in the bulk of the device, at node N, $E_N^{Fn} = E_N^{Fp} = 0$, i.e. $\Phi_N^n = \Phi_N^p = 1$.

To enforce that the quasi-Fermi levels remain continuous across heterointerfaces, one can modify the electrostatic potential V_i in the discretised current equations (7a) and (7b) by including the band offsets with respect to a reference material, in our case GaN. Hence, the potentials entering (7a) and (7b) are $V_i^n = V_i - \Delta E_i^c$ and $V_i^p = V_i - \Delta E_i^c + E_i^g$, respectively.

C. Schrödinger equation

When a voltage higher than the threshold voltage is applied at the gate of an AlGaN/GaN HEMT, the electrons become confined within a quantum well on the GaN-side of the heterointerface. Therefore, instead of using the classical expressions for the electron concentration given by Boltzmann or Fermi-Dirac statistics, a solution of the Schrödinger equation is necessary to obtain the quantised energy levels and electron wavefunctions from which the carrier concentration can be calculated. To this end, the 1D single-particle Schrödinger equation for Γ-valley electrons is solved within the effective mass approximation:

$$\left[-\frac{\hbar^2}{2qm^*(z)}\frac{\partial^2}{\partial z^2} + E_c(z)\right]\psi_n(z) = E_n\psi_n(z). \tag{11}$$

The discrete states E_n and wavefunctions $\psi_n(z)$ are then used to calculate the electron concentration in the following way (neglecting the non-parabolicity of the bands):

$$n(z) = \sum_n k_BT\frac{m^*(z)}{\pi\hbar^2}\ln\left[1+\exp\left(\frac{E_{Fn}(z)-E_n}{V_t}\right)\right]\psi_n^2(z). \tag{12}$$

D. Procedure for solving the full electrostatic problem

As mentioned previously, the Poisson equation, the two continuity equations and the Schrödinger equation are solved numerically in a self-consistent procedure to obtain the final solution of the electrostatic problem in question. A version of Gummel's iterative scheme [19] is used to this end. First of all, for an initial guess of the potential $V(z)$, the continuity equations are solved to obtain the quasi-Fermi levels $E_{Fn}(z)$ and $E_{Fp}(z)$. Thereafter, the Schrödinger equation is solved and (12) is used to obtain the electron concentration $n(z)$ for the given $E_{Fn}(z)$. Since quantum confinement of holes is not expected in the HEMT structures of interest, the hole concentration $p(z)$ can be obtained classically using Boltzmann or Fermi-Dirac statistics. The carrier concentrations $n(z)$ and $p(z)$ are then fed back into the Poisson equation and its solution provides a new guess for $V(z)$. The new potential is

then scaled using a linear mixing scheme with a variable damping parameter, and a new iteration starts by solving the continuity equations once again using the scaled $V(z)$. This procedure is repeated until the potential converges to within a set tolerance, typically 1 mV. Note that the quasi-Fermi levels are also scaled after solving the continuity equations to facilitate the convergence of the potential. If a sweep of the gate voltage is performed, it is convenient to use the solution of $V(z)$ at a given gate voltage as the initial guess for the next point in the sweep, which ensures fast convergence even at high gate biases. The material parameters for GaN and AlN used during the self-consistent calculations are listed in Table I, while the parameters for $Al_xGa_{1-x}N$ are interpolated as a linear function of x.

TABLE I: Material parameters for GaN and AlN used in the self-consistent calculations.

Parameter	Symbol	Material	Value	Unit
bandgap	E_g	GaN	3.42	eV
		AlN	6.13	
dielectric constant	ε	GaN	9.5	ε_0
		AlN	9	
effective electron mass	m_n^*	GaN	0.2	m_0
		AlN	0.49	
effective hole mass	m_p^*	GaN	1.5	
		AlN	7.26	
electron diffusion coefficient	D_n	GaN	25	cm^2/s
		AlN	7	
hole diffusion coefficient	D_p	GaN	5	
		AlN	0.3	

III. Simulations of an Enhancement-Mode HEMT

To demonstrate the functionality of the simulation procedure described in Sec. II, we simulate the electrostatics of a previously characterised enhancement-mode HEMT structure with a p-GaN cap. Chiu et al. [20] have shown that the performance of a standard p-GaN/AlGaN/GaN HEMT is improved by using a composite $AlN/Al_{0.17}Ga_{0.83}N/Al_{0.3}Ga_{0.7}N$ barrier instead of a conventional $Al_{0.17}Ga_{0.83}N$ barrier. Therefore, we choose to perform our simulations on the advanced composite-barrier structure, shown in Fig. 1. The 60 nm-thick p-GaN cap layer is used to deplete the 2DEG under the gate region at a zero gate bias, thereby achieving normally-off operation. This becomes clear when looking at the simulated band diagram along the 1D cutline in the z-direction at $V_G = 0$ V, which is shown in Fig. 2. The p-type doping in the cap layer lifts the conduction band in the GaN channel above the equilibrium Fermi-level at 0 eV and prevents the formation of the 2DEG. Therefore, a positive gate bias needs to be applied to achieve a high 2DEG concentration and switch the transistor on. The acceptor concentration in the Mg-doped cap is 3×10^{19} cm^{-3}, but due to the high activation energy of Mg in GaN, the concentration of activated Mg dopants at room temperature is measured to be 10^{18} cm^{-3} [20], which is the number used in our simulation. For the unintentionally doped AlGaN and GaN

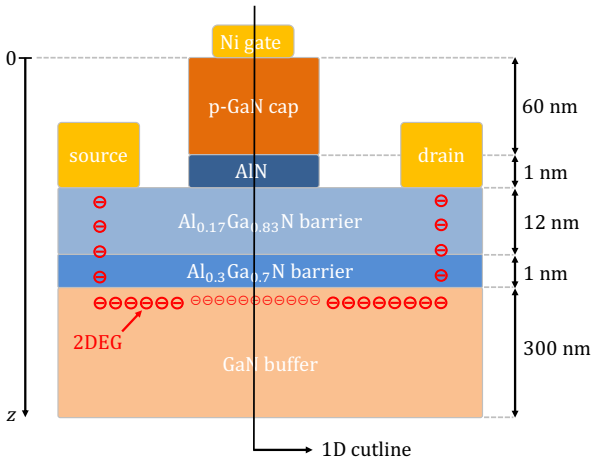

Fig. 1: 2D cross-section of the studied composite-barrier HEMT with a p-GaN cap. The 1D calculations are performed along the cutline in the z-direction.

layers, a background donor concentration of 10^{16} cm^{-3} is assumed. The Schottky barrier height of $\varphi_b^n = 1.46$ eV at the Ni gate contact is obtained using the Schottky-Mott rule and an electron affinity of 3.76 eV for the p-GaN material, as measured in [21].

Fig. 3 shows the gate voltage dependence of the electron sheet density, exhibiting the typical linear behaviour above the threshold voltage of 1.6 V, which matches the experimentally obtained value [22]. Fig. 3 also shows the dependence of the channel on-resistance in the region under the gate, calculated by dividing the gate length of 3 µm with $(qN_S\mu_{TOT})$, where N_S is the electron sheet density under the gate and μ_{TOT} is the total 2DEG mobility obtained using our mobility calculator, which is further described in Sec. IV.

For the structures fabricated using an optimised annealing process, an experimental value of 10.2 Ω·mm for the total on-resistance is obtained at a gate bias of 8 V [22]. To simulate the structure at such a high gate voltage, unlike

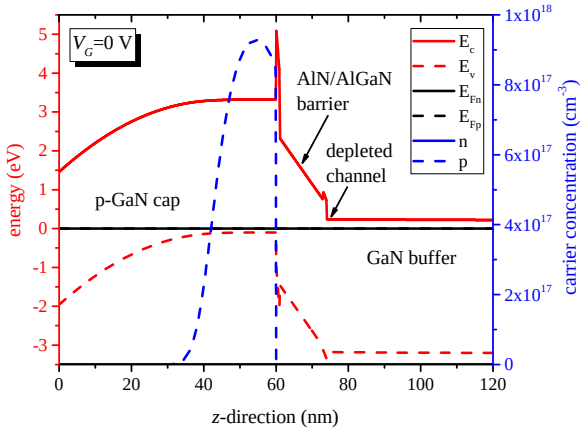

Fig. 2: Band diagram and carrier concentrations under the gate of the simulated HEMT structure at $V_G = 0$ V. The presence of the p-GaN cap layer depletes the 2DEG in the channel and results in enhancement-mode operation.

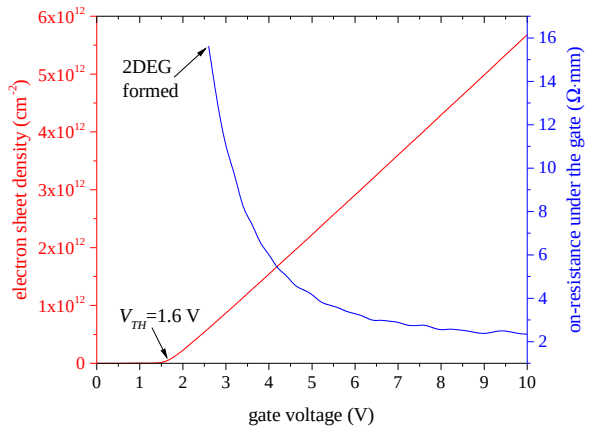

Fig. 3: Gate voltage dependence of the electron sheet density and on-resistance in the region under the gate. The threshold voltage of $V_{TH} = 1.6$ V matches the experimentally obtained value [22].

the simulation with $V_G = 0$ V shown in Fig. 2, the continuity equations need to be solved to obtain the position-dependent quasi-Fermi levels. To correctly reproduce the depletion behaviour of the p-GaN cap, one needs to solve the continuity equation for holes as well as electrons and include the free hole concentration in the Poisson equation, even though the HEMT itself is a unipolar device. The band diagram with $V_G = 8$ V is shown in Fig. 4. For the Poisson equation, we use a Neumann boundary condition in the bulk of the device, while for the quasi-Fermi levels at the gate contact, the boundary conditions given by (10a) and (10b) are used. The Schrödinger equation is solved only within the quantum well region, which extends 5 nm into the AlGaN barrier, so that wavefunction penetration into the barrier is taken into account. Having obtained the correct states and wavefunctions, we can estimate the total on-resistance by calculating μ_{TOT}. We assume that, at a gate bias of 8 V, the resistance of the source/drain access regions is similar to the on-resistance under the gate, which is reasonable since a 2DEG sheet density above $\sim 3\times10^{12}$ cm^{-2} is expected in the access regions, meaning that this resistance is close to its saturated value from Fig. 3. In that case, the total on-resistance is given simply by taking the total length of the device including the length of the gate and the access regions, which is equal to 12 μm, and dividing it by $(qN_S\mu_{TOT})$. Such a calculation gives a value of 10 Ω·mm for the total on-resistance at $V_G = 8$ V, which is very close to the experimental value of 10.2 Ω·mm. This suggests that the measured on-resistance of the structures fabricated using the optimised process is close to the theoretical limit and not impaired by contact resistances or other parasitic effects.

IV. Mobility Calculations

Further insight into the gate voltage dependence of the on-resistance can be gained by analysing the 2DEG mobility limited by various scattering mechanisms. Our mobility calculator [10], which builds on our previous work for III-V devices [23], [24], finds the mobility limited by all relevant scattering mechanisms, which are acoustic deformation potential scattering (ADP), piezoelectric scattering (PE), scattering by polar optical phonons (POP), alloy disorder scattering (ADO) in the AlGaN barrier, Coulomb scattering (CO) due to impurities, interface roughness scattering (IFR) and scattering due to dislocations (DIS). The scattering rates for each mechanism are obtained from the scattering matrix elements using Fermi's golden rule, and the MRTA is used to find the momentum relaxation rates and mobilities. Details of the mobility calculations for each mechanism have been described elsewhere [10]. All the scattering-related material parameters used in the calculations are also given in [10], with the exception of the RMS heterointerface roughness, which is taken as 1 Å. Fig. 5 shows the gate voltage dependence of the calculated room-temperature 2DEG mobility limited by the various scattering mechanisms. In the whole range of investigated gate voltages, the total mobility is limited mainly by POP scattering, which is typically the case for GaN-

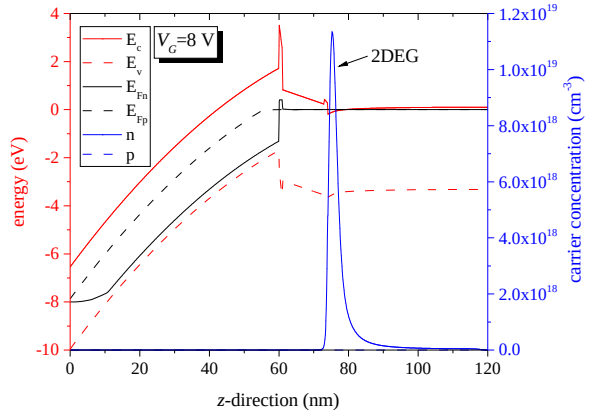

Fig. 4: Band diagram and carrier concentrations under the gate of the simulated HEMT structure at $V_G = 8$ V. The position-dependent quasi-Fermi levels are obtained by solving the continuity equations for both types of carriers.

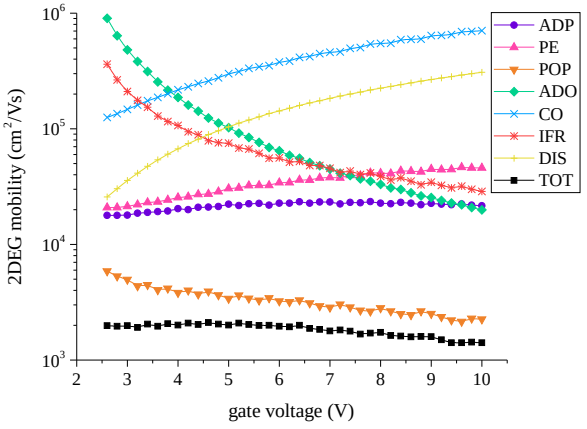

Fig. 5: Gate voltage dependence of the room-temperature 2DEG mobility limited by different scattering mechanisms for the GaN HEMT in Fig. 1. The POP-limited mobility is the dominant factor determining the total mobility, which shows a slight decrease due to stronger confinement at high gate voltages.

based HEMTs at high temperatures. Apart from that, ADO and IFR scattering also play a significant role at higher gate voltages, when the penetration of the ground-state wavefunction into the AlGaN barrier becomes prominent. The POP-limited mobility and therefore the total mobility exhibit a slight decrease with increasing gate voltage due to the stronger confinement of the 2DEG, with μ_{TOT} dropping from $\sim$2000 cm^2/Vs at $V_G = 2.6$ V, when the 2DEG is formed, to $\sim$1400 cm^2/Vs at $V_G = 10$ V. This is the reason for the saturation of the on-resistance with increasing gate bias in Fig. 3.

V. Conclusion

A simulation framework for modelling GaN-based HEMTs with high applied gate biases has been implemented in MATLAB. A self-consistent numerical procedure for solving the Schrödinger, Poisson and continuity equations for electrons and holes is used to accurately describe the electrostatics of arbitrary HEMT structures at arbitrary gate biases, and the calculated discrete states and wavefunctions are used in semi-classical calculations of the 2DEG mobility. The framework is demonstrated by simulating a previously characterised composite-barrier enhancement-mode HEMT with a p-GaN cap. A good match to experimental values of the threshold voltage and on-resistance is obtained, and the impact of different scattering mechanisms on the 2DEG mobility is analysed. We find that the decrease in mobility at high gate voltages leads to a saturation of the on-resistance with increasing gate bias.

References

[1] D. Jena, "Polarization induced electron populations in III-V nitride semiconductors: Transport, growth, and device applications," Ph.D. dissertation, University of California, Santa Barbara, 2003.

[2] K.-S. Lee, D.-H. Yoon, S.-B. Bae, M.-R. Park, and G.-H. Kim, "Self-consistent subband calculations of AlGaN/GaN single heterojunctions," *ETRI J.*, vol. 24, no. 4, pp. 270–279, 2002.

[3] J. Zhang, Y. Hao, J. Zhang, and J. Ni, "The mobility of two-dimensional electron gas in AlGaN/GaN heterostructures with varied Al content," *Sci. China Ser. F: Inf. Sci.*, vol. 51, no. 6, pp. 780–789, 2008.

[4] S. B. Lisesivdin, A. Yildiz, N. Balkan, M. Kasap, S. Ozcelik, and E. Ozbay, "Scattering analysis of two-dimensional electrons in AlGaN/GaN with bulk related parameters extracted by simple parallel conduction extraction method," *J. Appl. Phys.*, vol. 108, no. 1, p. 013712, 2010.

[5] A. Asgari, S. Babanejad, and L. Faraone, "Electron mobility, Hall scattering factor, and sheet conductivity in AlGaN/AlN/GaN heterostructures," *J. Appl. Phys.*, vol. 110, no. 11, p. 113713, 2011.

[6] K. Abgaryan, I. Mutigullin, and D. Reviznikov, "Theoretical investigation of 2DEG concentration and mobility in the AlGaN/GaN heterostructures with various Al concentrations," *Phys. Stat. Sol. C*, vol. 12, no. 12, pp. 1376–1382, 2015.

[7] I. Berdalovic, M. Poljak, and T. Suligoj, "On the modelling of interface roughness scattering in AlGaN/GaN heterostructures," in *43rd International Convention on Information, Communication and Electronic Technology*, Oct. 2020, pp. 29–34.

[8] M. N. Gurusinghe, S. K. Davidsson, and T. G. Andersson, "Two-dimensional electron mobility limitation mechanisms in $Al_xGa_{1-x}N$/GaN heterostructures," *Phys. Rev. B*, vol. 72, p. 045316, 2005.

[9] D. Y. Protasov, T. V. Malin, A. V. Tikhonov, A. F. Tsatsulnikov, and K. S. Zhuravlev, "Electron scattering in AlGaN/GaN heterostructures with a two-dimensional electron gas," *Semiconductors*, vol. 47, no. 1, pp. 33–44, 2013.

[10] I. Berdalovic, M. Poljak, and T. Suligoj, "A comprehensive model and numerical analysis of electron mobility in GaN-based high electron mobility transistors," *J. Appl. Phys.*, vol. 129, no. 6, p. 064303, 2021.

[11] D. Vasileska, S. M. Goodnick, and G. Klimeck, *Computational Electronics: Semiclassical and Quantum Device Modeling and Simulation*. Boca Raton, FL, USA: CRC Press, 2010.

[12] O. Ambacher *et al.*, "Two dimensional electron gases induced by spontaneous and piezoelectric polarization undoped and doped AlGaN/GaN heterostructures," *J. Appl. Phys.*, vol. 87, no. 1, pp. 334–344, 2000.

[13] D. L. Scharfetter and H. K. Gummel, "Large-signal analysis of a silicon Read diode oscillator," *IEEE Trans. Electron Devices*, vol. 16, no. 1, pp. 64–77, 1969.

[14] *A Manual for AMPS-1D: A One-Dimensional Device Simulation Program for the Analysis of Microelectronic and Photonic Structures*, Center for Nanotechnology Education and Utilization, Pennsylvania State University, University Park, PA, USA, 2010.

[15] J. W. Slotboom, "Computer-aided two-dimensional analysis of bipolar transistors," *IEEE Trans. Electron Devices*, vol. 20, no. 8, pp. 669–679, 1973.

[16] S. Selberherr, *Analysis and Simulation of Semiconductor Devices*. Vienna, Austria: Springer, 1984.

[17] A. Iqbal and K. Bevan, "Simultaneously solving the photovoltage and photocurrent at semiconductor-liquid interfaces," *J. Phys. Chem. C*, vol. 122, no. 1, pp. 30–43, 2017.

[18] J. Nylander, F. Masszi, S. Selberherr, and S. Berg, "Computer simulations of Schottky contacts with a non-constant recombination velocity," *Solid-State Electron.*, vol. 32, no. 5, pp. 363–367, 1989.

[19] H. K. Gummel, "A self-consistent iterative scheme for one-dimensional steady state transistor calculations," *IEEE Trans. Electron Devices*, vol. 11, no. 10, pp. 455–465, 1964.

[20] H. Chiu *et al.*, "High-performance normally off p-GaN gate HEMT with composite AlN/$Al_{0.17}Ga_{0.83}$N/$Al_{0.3}Ga_{0.7}$N barrier layers design," *IEEE J. Electron Devices Soc.*, vol. 6, pp. 201–206, 2018.

[21] Y.-J. Ji, Y.-J. Du, and M.-S. Wang, "Electron affinity of GaN(0001) surface doped with Al, Mg," *Optik*, vol. 127, no. 7, pp. 3624–3628, 2016.

[22] H. Chiu *et al.*, "Dynamic behavior improvement of normally-off p-GaN high-electron-mobility transistor through a low-temperature microwave annealing process," *IEEE J. Electron Devices Soc.*, vol. 7, pp. 984–989, 2019.

[23] M. Poljak, V. Jovanovic, D. Grgec, and T. Suligoj, "Assessment of electron mobility in ultrathin-body InGaAs-on-insulator MOSFETs using physics-based modeling," *IEEE Trans. Electron Devices*, vol. 59, no. 6, pp. 1636–1643, 2012.

[24] S. Krivec, M. Poljak, and T. Suligoj, "The physical mechanisms behind the strain-induced electron mobility increase in InGaAs-on-InP MOSFETs," *IEEE Trans. Electron Devices*, vol. 65, no. 7, pp. 2784–2789, 2018.